IEEE Transactions on Industry Applications, Vol. 38, No. 4, July/Aug 2002, pp. 1087-1095

Sensorless Vector Control of Induction Motors at Very Low Speed using a Nonlinear Inverter Model and Parameter Identification

Joachim Holtz, *Fellow, IEEE*, and Juntao Quan
University of Wuppertal
42097 Wuppertal – Germany

Abstract — **The performance of vector controlled induction motor drives without speed sensor is generally poor at very low speed. The reasons are offset and drift components in the acquired feedback signals, voltage distortions caused by the nonlinear behavior of the switching converter, and the increased sensitivity against model parameter mismatch.**

New modeling and identification techniques are proposed to overcome these problems. A pure integrator is employed for stator flux estimation which permits high estimation bandwidth. Compensation of the drift components is done by offset identification. The nonlinear voltage distortions are corrected by a self-adjusting inverter model. A further improvement is a novel method for online adaptation of the stator resistance. Experiments demonstrate smooth steady-state operation and high dynamic performance at extreme low speed.

1. Introduction

Controlled induction motor drives without speed sensor have developed as a mature technology in the past few years. However, their performance at very low speed is poor. The main reasons are the limited accuracy of stator voltage acquisition, the presence of offset and drift components in the acquired voltage signals, their limited bandwidth, offsets and unbalances in the current signals, and the increased sensitivity against model parameter mismatch.

These deficiencies degrade the accuracy of flux estimation at low speed. The dynamic performance of a sensorless drive then deteriorates. Sustained operation at very low speed becomes impossible as ripple components appear in the machine torque and the speed starts oscillating, eventually leading to instable operation of the system.

2. Sources of Inaccuracy and Instability

2.1 Estimation of the flux linkage vector

Most sensorless control schemes rely directly or indirectly on the estimation of the stator flux linkage vector $\boldsymbol{\psi}_s$ [1, 2], being defined as the time integral of the induced voltage,

$$\hat{\boldsymbol{\psi}}_s = \int \left(\hat{\boldsymbol{u}}_s - \hat{r}_s \boldsymbol{i}_s + \boldsymbol{u}_{off}\right) d\tau , \qquad (1)$$

where $\boldsymbol{u}_s$ is the stator voltage vector, $\boldsymbol{i}_s$ is the stator current vector and r_s is the stator resistance. Time is normalized as $\tau = \omega_{sR} t$, where ω_{sR} is the nominal stator frequency [3]. The added symbol $\hat{}$ marks estimated variables. The vector $\boldsymbol{u}_{off}$ in (1) represents all disturbances such as offsets, unbalances and other errors that are contained in the estimated induced voltage $\hat{\boldsymbol{u}}_i = \hat{\boldsymbol{u}}_s - \hat{r}_s \boldsymbol{i}_s$, resulting from either the voltage signal $\hat{\boldsymbol{u}}_s$ or from the current signal $\boldsymbol{i}_s$. A major source of error is a mismatch of the model parameter r_s.

Rotor flux oriented schemes estimate the rotor flux linkage vector as

$$k_r \hat{\boldsymbol{\psi}}_r = \int (\hat{\boldsymbol{u}}_s - \hat{r}_s \boldsymbol{i}_s + \boldsymbol{u}_{off})\, d\tau - \hat{\sigma} \hat{l}_s \boldsymbol{i}_s = \hat{\boldsymbol{\psi}}_s - \hat{\boldsymbol{\psi}}_\sigma \qquad (2)$$

where $k_r = l_h / l_r$ is the coupling factor of the rotor windings, $\sigma = 1 - l_m^2 / l_s l_r$ is the total leakage factor, l_m is the mutual inductance between the stator and rotor windings, l_s is the stator inductance, and l_r is the rotor inductance. $\boldsymbol{\psi}_\sigma$ is the total leakage flux vector.

The estimation of one of the flux vectors according to (1) or (2) requires performing an integration in real-time. The use of a pure integrator has not been reported in the literature. The reason is that an integrator has an infinite gain at zero frequency. The unavoidable offsets contained in the integrator input then make its output gradually drift away beyond limits. Therefore, instead of an integrator, a low pass filter usually serves as a substitute. A low pass filter has a finite dc gain which eases the drift problem, although drift is not fully avoided. However, a low pass filter introduces severe phase angle and amplitude errors at frequencies around its corner frequency, and even higher errors at lower frequencies. Its corner frequency is normally set to 0.5 - 2 Hz, depending on the existing amount of offset. The drive performance degrades below stator frequencies 2 - 3 times this value; the drive becomes instable at speed values that correspond to the corner frequency.

Different ways of compensating the amplitude and phase angle errors at low frequencies have been proposed [4 - 7]. Ohtani [4] reconstructs the phase angle and amplitude error produced by the low pass filter. A load dependent flux vector reference is synthesized for this purpose. This signal is transformed to stator coordinates and then passed through a second low pass filter having the same time constant. The resulting error vector is added to the erroneous flux estimate. Although the benefits of this method are not explicitly documented in [4], improved performance should be expected in an operating range around the corner frequency of the low pass filter.

With a view to improving the low speed performance of flux estimation, Shin et. al. [5] adjust the corner frequency of the low pass filter in proportion to the stator frequency, while compensating the phase and gain errors by their respective steady-state values. It was not demonstrated, though, that dynamic operation at very low frequency is improved. Hu and Wu [6] try to force the stator flux vector onto a circular trajectory by PI control. While this can provide a correct result in the steady-state, it is erroneous at transient operation and also exhibits a large error at start-up. A practical application of this method has not been reported; our investigations show loss of field orientation following transients.

2.2 Acquisition of the stator voltages

The induced voltage, which is the signal to be integrated for flux vector estimation, is obtained as the difference between the stator voltage and the resistive voltage drop across the machine windings. When a voltage source inverter (VSI) is used to feed the machine, the stator voltages are formed by pulse trains having a typical rise time of 2 - 10 kV/μs. These are digitally acquired at a high, though limited sampling rate [7]. The limited bandwidth of such sampling process may fail to establish the exact volt-second equivalent between the actual and the acquired signals, and hence produce an error. To avoid this complication, some authors have used a current source inverter (CSI) [6], or a linear power amplifier [8], to make use of smooth voltage waveforms that can be accurately acquired even at limited sampling rate.

To avoid this problem in a switched VSI drive, it is preferred to replace the actual stator voltages by the reference voltage vector that controls the pulsewidth modulator, $\boldsymbol{u}^* \approx \boldsymbol{u}_{s1}$, where $\boldsymbol{u}_{s1}$ is the fundamental component of $\boldsymbol{u}_s$. This very simple method yields good results, except when operating in the low speed region. The respective magnitudes u_s and u_i are then very small and the errors may even exceed the actual signals in magnitude. One of the predominant sources of error at very low speed is the nonlinear relationship between $\boldsymbol{u}^*$ and $\boldsymbol{u}_{s1}$ caused by the switching characteristics of the inverter.

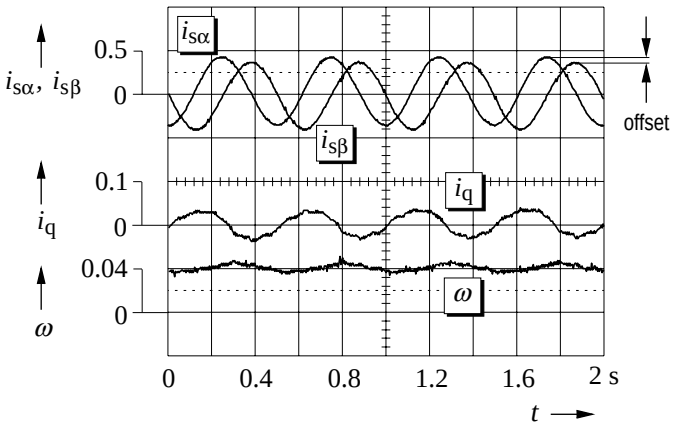

Fig. 1. The effect of a dc offset in one of the current signals on the performance of a vector controlled drive system

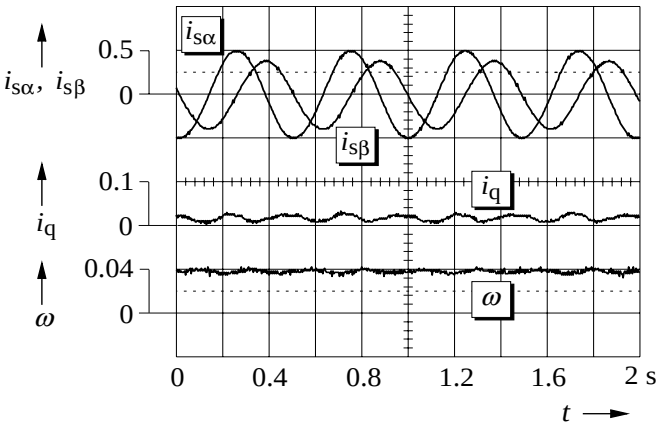

Fig. 2. The effect of a gain unbalance between the acquired current signals on the performance of a vector controlled drive

2.3 Acquisition of the stator currents

The stator currents are usually measured by two Hall sensors. They are acquired as analog signals, which are subsequently digitized using A/D converters. The sources of errors in this process are dc offsets and gain unbalances in the analog signal channels [9]. After the transformation of the current signals to synchronous coordinates, dc offsets generate ac ripple components of fundamental frequency, while gain unbalances produce elliptic current trajectories instead of circular trajectories. The disturbance in the latter case is a signal of twice the fundamental frequency.

The following oscillograms demonstrate the effect of such disturbances on the performance of a vector controlled drive system. The respective disturbances are intentionally introduced, for better visibility at a higher signal level than would normally be expected in a practical implementation.

Fig. 1 shows the effect of 5% dc offset in one of the current signals on the no-load waveform of the *q*-axis current, and on the mechanical angular velocity ω. The drive is operated is at a stator frequency of 2 Hz. The transformed current signals generate oscillations in the torque producing current i_q. Resulting from this are torque pulsations of 0.06 nominal value, and corresponding oscillations in the speed signal ω. Note that nominal torque at rated flux is produced by $i_q = \cos \varphi$, were $\cos \varphi$ is the power factor of the motor.

Fig. 2 shows the same signals under the influence of 5% gain unbalance between the two current channels. Oscillations of twice the stator frequency are generated in the torque producing current, and also in the speed signal.

2.4 Estimation of the stator resistance

Another severe issue, in addition to the integration problem and to the nonlinear behavior of the of the inverter, is the mismatch between the machine parameters and the respective model parameters. In particular, adjusting the stator resistance $\hat{r}_s$ in (1) and (2) to match its actual value is most important for accurate stator flux estimation, and for stable operation at very low speed. The actual value of r_s varies

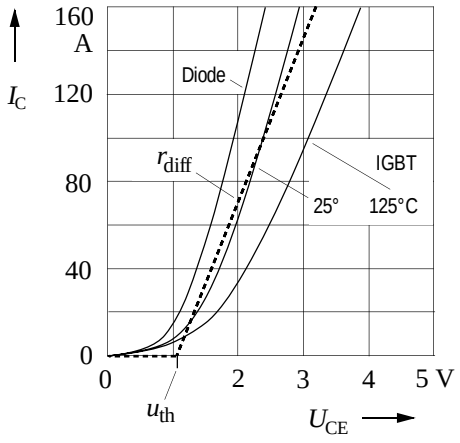

Fig. 3. Forward characteristics of the power devices

typically in a range of about 1 : 2 due to variations of the winding temperature. It is therefore apparent from (1) and (2) that the influence of the resistive voltage drop $\hat{r}_s\, i_s$, and hence of $\hat{r}_s$, becomes predominant when the magnitude u_s is small, i. e. at low speed. The stator current magnitude i_s ranges typically between 0.3 at no load and unity at nominal load.

Viewing the recent literature, the stator resistance is determined in [10] as the small difference between two large quantities, namely real stator power and airgap power, and as such the result is prone to error. The method presented in [11] relies on the accuracy of other machine parameters which are not necessarily constant, such as slip, leakage inductance and rotor resistance.

To overcome the aforementioned problems, this paper employs a pure integrator for stator flux estimation. Increased accuracy is achieved by eliminating direct stator voltage measurement. The available reference voltage signal is used instead, corrected by a self-adjusting nonlinear inverter model. A third improvement is a novel method for on-line adaptation of the stator resistance.

3. Models for Very Low Speed Operation

3.1 The inverter model

At very low speed, the voltage drop in the PWM inverter can be higher than the induced voltage, and hence constitutes a severe disturbance. The forward characteristics of the power devices are shown in Fig. 3. They can be modeled by an average threshold voltage u_{th} and an average differential resistance r_d [12]. The variations with temperature of the threshold voltage u_{th} are neglected in a first step. Thus, the approximated forward characteristics of the power devices are marked by the dotted line in Fig. 3.

A model of the inverter is derived considering the inverter topology during a switching sequence of one half cycle as shown in Fig. 4. The three phase currents i_a, i_b and i_c flow either through an active device, mostly an IGBT, or a recovery diode, depending on the switching state of the inverter. The directions of the phase currents, however, do not change in a larger time interval of about one sixth of a fundamental cycle. They depend only on the stator current vector $\boldsymbol{i}_s$. Fig. 4 illustrates that the effect of the device voltage drops does not change as the switching states change during pulsewidth modulation, provided that the directions of current flow do not change. The inverter then introduces voltage components u_{CE} of about equal magnitude to all the three phases, and it is the directions of the respective phase currents that determine their signs.

The device threshold voltage u_{th} as defined in Fig. 3 constitutes one portion of the device forward voltage. Its influence can be described by the threshold voltage vector

$$\boldsymbol{u}_{th} = \frac{1}{2}\left(u_{th}\mathrm{sign}(i_a) + \mathrm{a}\, u_{th}\mathrm{sign}(i_b) + \mathrm{a}^2 u_{th}\mathrm{sign}(i_c)\right), \qquad (3)$$

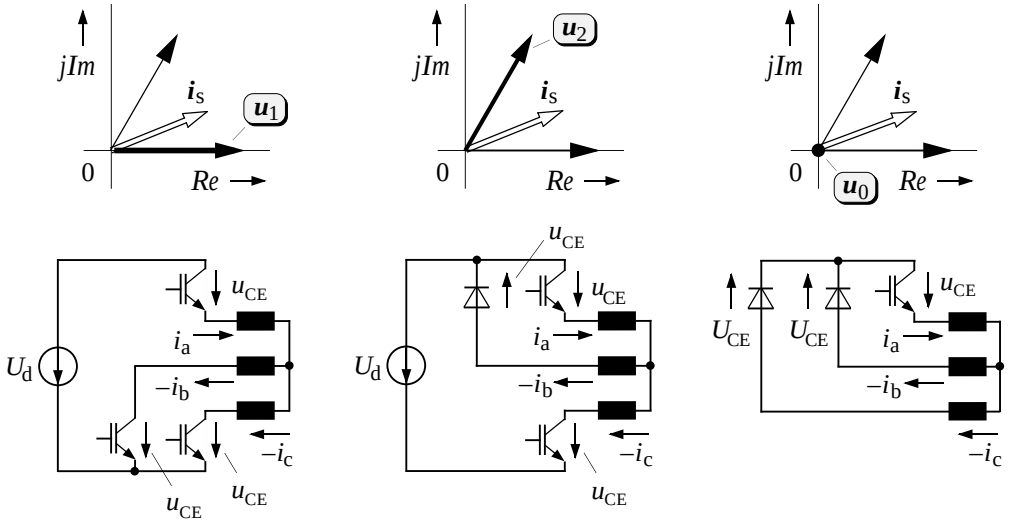

(a) switching state S_1 (b) switching state S_2 (c) switching state S_0

Fig. 4. Effect at pulsewidth modulation of the forward voltages u_{CE} of the power semiconductors

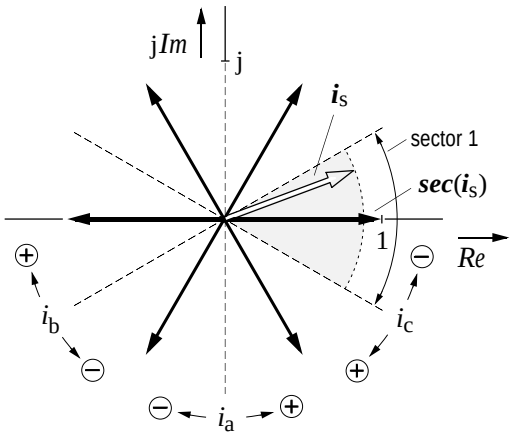

Fig. 5. The six possible locations of the sector indicator $\boldsymbol{sec}(\boldsymbol{i}_s)$; the dotted lines indicate the transitions at which the signs of the respective phase currents change

where a = $exp(j2\pi/3)$.

Equation (3) converts into

$$\boldsymbol{u}_{th} = u_{th} \cdot \boldsymbol{sec}(\boldsymbol{i}_s), \tag{4}$$

where

$$\boldsymbol{sec}(\boldsymbol{i}_s) = \frac{1}{2}\left(\text{sign}(i_a) + a\,\text{sign}(i_b) + a^2\text{sign}(i_c)\right) \tag{5}$$

is a nonlinear function of the stator current vector $\boldsymbol{i}_s(t)$. The sector indicator $\boldsymbol{sec}(\boldsymbol{i}_s)$ is a unity vector that indicates the respective ±30°-sector in which $\boldsymbol{i}_s$ is located. Fig. 5 illustrates the six possible locations of the sector indicator $\boldsymbol{sec}(\boldsymbol{i}_s)$ in the complex plane. The locations are determined by the respective signs of the three phase currents in (3), or, in other words, by a maximum of ±30° phase displacement between the vectors $\boldsymbol{i}_s$ and $\boldsymbol{sec}(\boldsymbol{i}_s)$.

The reference signal $\boldsymbol{u}^*$ of the pulsewidth modulator controls the stator voltage of the machine. It follows a circular trajectory in the steady-state. Owing to the forward voltages of the power devices, the average value $\boldsymbol{u}_{av}$ of the stator voltage vector $\boldsymbol{u}_s$, taken over a switching cycle, describes trajectories that result distorted and discontinuous. Fig. 6 shows that the fundamental amplitude of $\boldsymbol{u}_{av}$ is less than its reference value $\boldsymbol{u}^*$ at motoring, and larger at regeneration. The voltage trajectories exhibit strong sixth harmonic components in addition. Since the threshold voltage does not vary with frequency as the stator voltage does, the distortions are more pronounced at low stator frequency where the stator voltage is low. The distortions introduced by the inverter may even exceed the commanded voltage in magnitude, which then makes correct flux estimation and stable operation of the drive impossible.

Using the definitions (3) - (5), an estimated value $\hat{\boldsymbol{u}}_s$ of the stator voltage vector can be obtained from the PWM reference voltage vector $\boldsymbol{u}^*$

$$\hat{\boldsymbol{u}}_s = \boldsymbol{u}^* - \boldsymbol{u}_{th} - r_d\boldsymbol{i}_s, \tag{6}$$

where the two substracted vectors represent the total inverter voltage vector. The inverter voltage vector reflects the respective influence of the threshold voltages through $\boldsymbol{u}_{th}$, and of the resistive voltage drops of the power devices through $r_d\boldsymbol{i}_s$. A signal flow graph of the inverter model (6) is shown in the left hand side of Fig. 10.

3.2 Identification of the inverter model parameters

The threshold voltage u_{th} is one parameter of the inverter model. It is determined during a self-commissioning process from the distortions of the reference voltage vector $\boldsymbol{u}^*$. The components u_α^* and u_β^* of the reference voltage vector are acquired while using the current controllers to inject sinusoidal currents of very low frequency into the stator windings. In such condition, the machine impedance is dominated by the stator resistance. The stator voltages are then proportional to the stator currents. Any deviation from a sinewave of the reference voltages that control the pulsewidth modulator are therefore caused by the inverter.

As an example, an oscillogram of the distorted reference voltage waveforms u_α^* and u_β^*, measured at sinusoidal currents of magnitude i_s = 0.5, is shown in Fig. 7. The amplitude of the fundamental voltage is very low which is owed to the low frequency of operation. The distortions of the voltage waveforms in Fig. 7 are therefore fairly high. They are predominantly caused by the dead time effect of the inverter. Using such distorted voltages to represent the stator voltage signal in a stator flux estimator would lead to stability problems at low speed. Accurate inverter dead time compensation [13] is therefore mandatory for high performance applications.

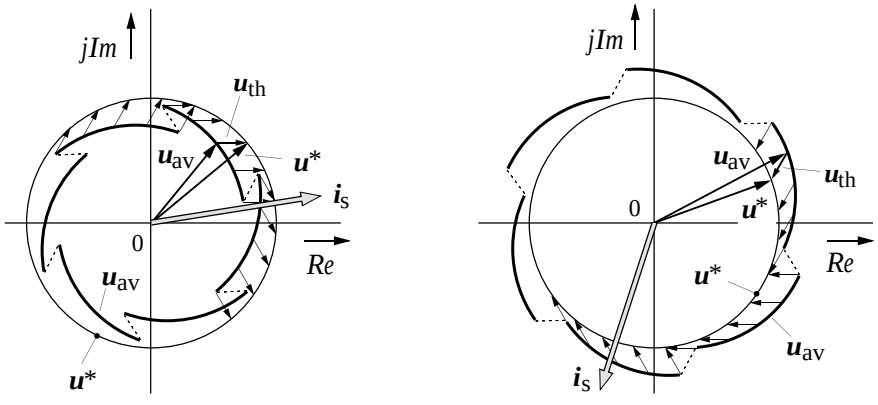

(a) at motoring (b) at regeneration

Fig. 6. The effect of inverter nonlinearity. The trajectory $\boldsymbol{u}_{av}$ represents the average stator voltage (switching harmonics excluded)

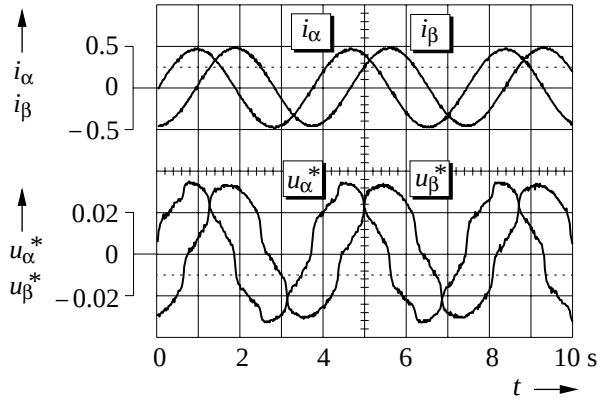

Fig. 7. The effect of inverter dead time on the components of the voltage vector $\boldsymbol{u}^*$, operation with injected sinewave currents, stator frequency 0.25 Hz

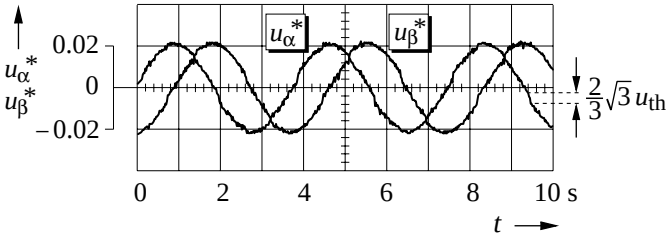

Fig. 8. Components of the reference voltage vector $\boldsymbol{u}^*$ as in Fig. 7, inverter operated with dead time compensation

Fig. 8 shows the same components of the reference voltage vector $\boldsymbol{u}^*$ with a dead time compensator implemented. The distortions are now much smaller, but complete linearity between the reference voltage vector $\boldsymbol{u}^*$ and the stator voltage vector $\boldsymbol{u}_s$ is not yet achieved. The remaining periodic step changes in the voltage waveforms are caused by the threshold voltages of the power devices, as described by (4) and illustrated in Fig. 6.

In Fig. 6, the step changes that characterize the distorted voltage trajectory have different magnitudes, as have the projections of the step changes on the respective axes. These are proportional to the sector indicator $\boldsymbol{sec}(\boldsymbol{i}_s)$ according to (4); the loscations of $\boldsymbol{sec}(\boldsymbol{i}_s)$ are shown in Fig. 4. It follows from (4) that both the larger step change and the amplitude of u_α^* have the magnitude $4/3\,u_{th}$ as indicated in Fig. 9.

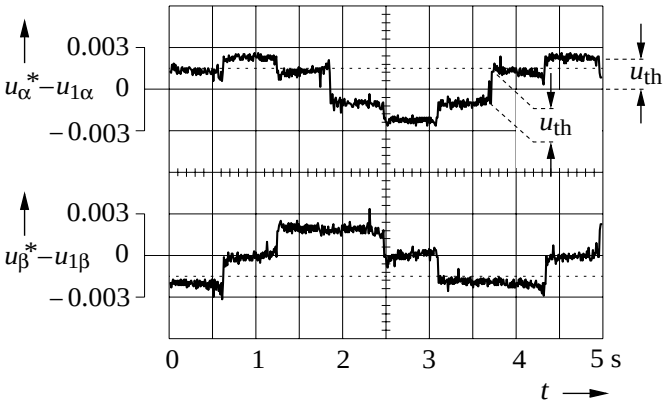

Fig. 9. The distortion voltage generated by the inverter; components in stationary coordinates

Extracting the value of the threshold voltage u_{th} from the waveform of u_α^* (or u_β^*) in Fig. 8 appears quite inaccurate. A better method is substracting the fundamental component u_{s1} from, e. g. u_α^*, which then yields a square wave like, stepped waveform as shown in Fig. 9. The fundamental component is easily extracted from a set of synchronous samples of u_α^* by Fast Fourier Transform.

The differential resistance of the power devices, r_d in (6), establishes a linear relation between the load current and its influence on the inverter voltage. Functionally, it adds to the resistance r_s of the stator windings and hence influences also upon the transient stator time constant of the induction motor, and on the design parameters of the current controllers. The value $(r_s + r_d)$ is estimated by an on-line tuning process described in Section 3.4.

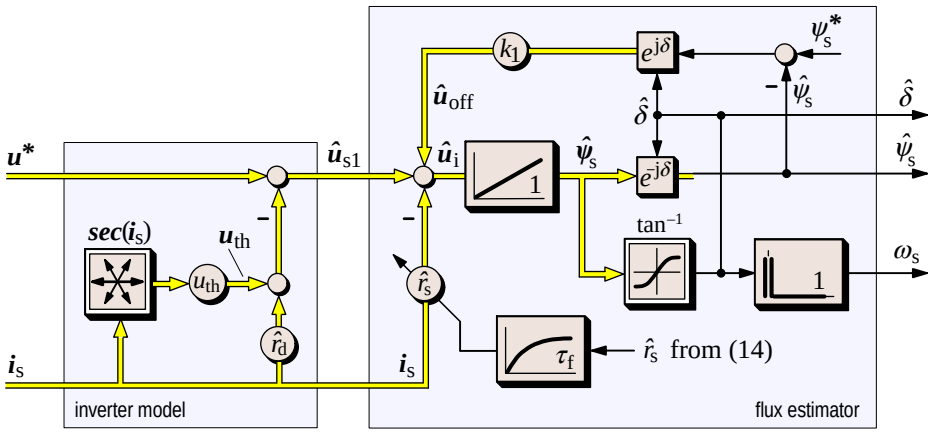

Fig. 10. Signal flow graph of the inverter model and the stator flux estimator

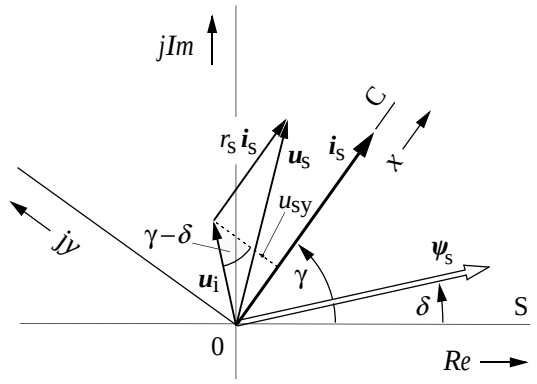

Fig. 11. Vector diagram illustrating the estimation of the stator resistance; S marks stationary reference frame (α,β) and C marks the current reference frame (x,y)

3.3 Stator flux estimation

The inverter model (6) is used to compensate the nonlinear distortions introduced by the power devices of the inverter. The model estimates the stator voltage vector $\boldsymbol{u}_s$ that prevails at the machine terminals, using the reference voltage vector $\boldsymbol{u}^*$ of the pulsewidth modulator as the input variable. The inverter model thus enables a more accurate estimation of the stator flux linkage vector. The signal flow graph of the inverter model is shown in the left hand side of Fig. 10.

The right hand side of Fig. 10 shows the signal flow graph of the stator flux estimator. It is a particular attraction of this approach that the stator flux vector is obtained by pure integration. The method necessarily incorporates the estimation of a time-varying vector that must represent the offset voltages. Implementing a pure integrator avoids the usual estimation errors and bandwidth limitation associated with using a low pass filter. This is a particular advantage when operating at very low frequency.

The defining equation of the stator flux estimator is

$$\hat{\boldsymbol{\psi}}_s = \int (\hat{\boldsymbol{u}}_s - \hat{r}_s \boldsymbol{i}_s + \hat{\boldsymbol{u}}_{off})\, d\tau \tag{7}$$

where $\hat{\boldsymbol{u}}_s$ is the estimated stator voltage vector, and

$$\hat{\boldsymbol{u}}_{off} = k_1 \left(\psi_s^* - \hat{\psi}_s \right) e^{j\hat{\delta}} \tag{8}$$

is the estimated effective offset voltage vector, while $\hat{\delta}$ is the estimated stator field angle. The offset voltage vector $\hat{\boldsymbol{u}}_{off}$ in (7) is determined such that the estimated stator flux vector $\hat{\boldsymbol{\psi}}_s$ rotates close to a circular trajectory in the steady-state, which follows from (7) and from the right hand side of (8).

To enable the identification of $\hat{\boldsymbol{u}}_{off}$ in (8), the stator field angle $\hat{\delta}$ is estimated as

$$\hat{\delta} = tan^{-1}\left(\frac{\hat{\psi}_{sq}}{\hat{\psi}_{sd}} \right), \tag{9}$$

as illustrated in the right portion of Fig. 10. The magnitude of the stator flux linkage vector is then obtained as

$$\hat{\psi}_s = \hat{\boldsymbol{\psi}}_s\, e^{-j\hat{\delta}}. \tag{10}$$

This value is used in (8) to determine the vector of the effective offset voltage.

The gain constant k_1 in (8) is chosen such that the ac disturbances introduced by dc offsets and unbalanced gains of the stator current acquisition channels are well compensated. Values in the range $k_1 = 0.4 \ldots 0.8$ serve this purpose in a satisfactory manner.

The stator frequency signal is computed by

$$\omega_s = \frac{d\hat{\delta}}{d\tau}, \tag{11}$$

from which the angular mechanical velocity ω is determined, for instance with reference to [2]:

$$\hat{\omega} = \omega_s - \hat{\omega}_r = \omega_s - \frac{l_s}{\tau_r} \frac{\tau'_r \frac{di_q}{d\tau} + i_q}{\psi_s - \sigma l_s i_{sd}}. \tag{12}$$

3.4 Stator resistance estimation

Utilizing the inherent good low-speed performance of the novel flux estimator requires the accurate on-line adaptation of the stator resistance, which is the relevant parameter of the machine model. The proposed algorithm relies on the orthogonal relationship in steady-state between the stator flux vector and the induced voltage. The inner product of these two vectors is

$$\hat{\boldsymbol{\psi}}_s \circ \hat{\boldsymbol{u}}_i = \hat{\boldsymbol{\psi}}_s \circ (\hat{\boldsymbol{u}}_s - \hat{r}_s \boldsymbol{i}_s). \tag{13}$$

This expression depends on the stator resistance. To reduce the on-line computation time for its estimation, (13) is transformed to a reference frame that aligns with the current vector. This current reference frame (*xy*-frame) rotates in synchronism and is displaced with respect to stationary coordinates by the phase angle $\gamma(\tau)$ of the stator current, as shown in Fig. 11. We have $\boldsymbol{i}_s^{(C)} = \boldsymbol{i}_s^{(S)} \cdot \exp(-j\gamma)$ and consequently $i_{sx} = i_s$ and $i_{sy} = 0$. Of the superscripts, $^{(S)}$ refers to stator coordinates and $^{(C)}$ refers to current coordinates.
The estimated value of the stator resistance is obtained as the solution of (13) in current coordinates

$$\hat{r}_s = \frac{\hat{u}_{sx} - \frac{\hat{\psi}_{sy}}{\hat{\psi}_{sx}} \hat{u}_{sy}}{i_{sx}} = \frac{\hat{u}_{sx} - \omega_s \tilde{\psi}_s \sin\left(\gamma - \hat{\delta}\right)}{i_s} \tag{14}$$

using the relationships

$$\frac{\hat{\psi}_{sy}}{\hat{\psi}_{sx}} = tan\left(\gamma - \hat{\delta}\right) \tag{15}$$

and

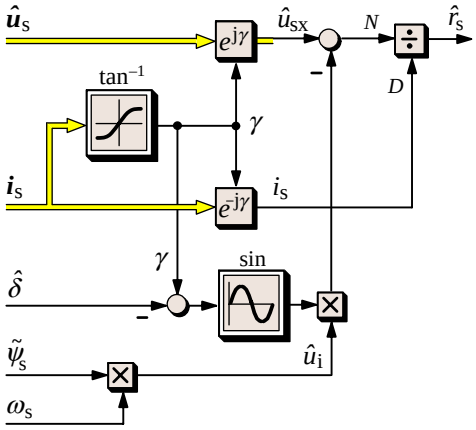

Fig. 12. Signal flow graph of the stator resistance estimator

$$u_{sy} = \hat{u}_i \cos\left(\gamma - \hat{\delta}\right), \tag{16}$$

which can be taken from the vector diagram Fig 10. Furthermore, we have in a steady-state

$$\hat{u}_i = \omega\, \tilde{\psi}_s \tag{17}$$

were $\tilde{\boldsymbol{\psi}}_s$ is an estimated stator flux value defined by (20).

The signal flow diagram of the stator resistance adaptation scheme is shown in Fig. 12.

The value of $\tilde{\boldsymbol{\psi}}_s$ in (17) cannot be obtained from the stator flux estimator Fig. 10, equation (7), as it would be erroneous if the modeled value $\hat{r}_s$ of the stator resistance is wrongly identified. Another estimated value, $\tilde{\boldsymbol{\psi}}_s$, is therefore used, being derived from the instantaneous reactive power $\boldsymbol{u}_s \times \boldsymbol{i}_s|_z$. This notation describes the *z*-component of the vector product of the stator voltage and current vectors.

The system equation, for example given in [3], is

$$\tau_{sr}{}' \frac{d\boldsymbol{i}_s}{d\tau} + \boldsymbol{i}_s = -\,\mathrm{j}(\omega_s - \omega)\tau_{sr}{}' \boldsymbol{i}_s + \frac{1}{r_{sr}}\left(\frac{1}{\tau_r} - \mathrm{j}\omega\right)\boldsymbol{\psi}_s + \frac{1}{r_{sr}}\boldsymbol{u}_s \tag{18}$$

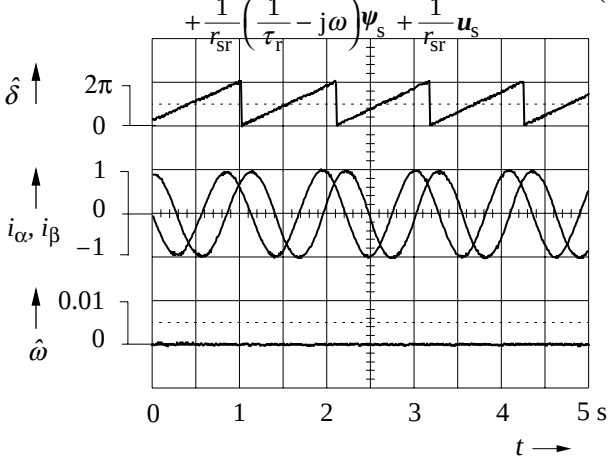

Fig. 13. Zero speed operation at steady-state and nominal load, 0.9 Hz stator frequency

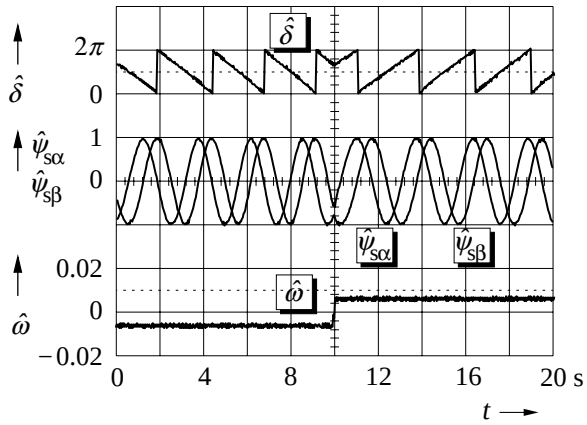

Fig. 14. Speed reversal at 10 rpm, fundamental frequency $f_1 = \omega_s/2\pi = \pm 0.33$ Hz

were $\tau_{sr}{}' = \sigma l_s/(r_s + k_r r_r)$. Equation (18) is externally multiplied by the vector $\boldsymbol{i}_s$, from which

$$\boldsymbol{u}_s \times \boldsymbol{i}_s - \sigma l_s \frac{d\boldsymbol{i}_s}{d\tau} \times \boldsymbol{i}_s - \mathrm{j}\omega\sigma l_s \boldsymbol{i}_s \times \boldsymbol{i}_s = \left(\mathrm{j}\omega - \frac{1}{\tau_r}\right)\boldsymbol{\psi}_s \times \boldsymbol{i}_s \tag{19}$$

is obtained. This operation eliminates the stator and the rotor resistances from (18) where these parameters are there contained in $\tau_{sr}{}'$. Taking the *z*-component of all terms in (19) and assuming field orientation, $\psi_{sd} = \psi_s$ and $\psi_{sd} = 0$, we have

$$\tilde{\psi}_s = \frac{\left(u_{sq} i_d - u_{sd} i_q\right) - \omega\sigma l_s i_s{}^2 + \sigma l_s\left(i_q \frac{di_d}{d\tau} - i_d \frac{di_q}{d\tau}\right)}{\omega\, i_d + \frac{i_q}{\tau_r}} \tag{20}$$

The stator flux value thus obtained does not depend on the stator resistance. It is used in the stator resistance estimator Fig. 12 to compute the magnitude of the induced voltage.

The stator flux vector as estimated by (20) depends on the total leakage inductance σl_s as the only uncertain parameter. Its contribution to (20) represents the total leakage flux linkages and their changes with time. An error in σl_s has only a marginal effect on $\tilde{\psi}_s$ since the total leakage flux makes up for about only 10% of the stator flux at nominal load.

The estimated stator resistance value $\hat{r}_s$ from (14) is used as an input signal to the stator flux estimator Fig. 10. It adjusts its parameter through a low pass filter. The non-normalized value of the filter time constant τ_f is about 100 ms.

4. Experimental Results

The system was implemented in a 11-kW PWM inverter fed induction motor drive. The machine data are: 380 V, 22 A, 1460 rpm. A controlled dc machine was used as the load.

The oscillogram Fig. 13 shows zero speed operation in the steady-state at 0.9 Hz stator frequency and nominal load. The stator currents are exactly sinusoidal and the commanded

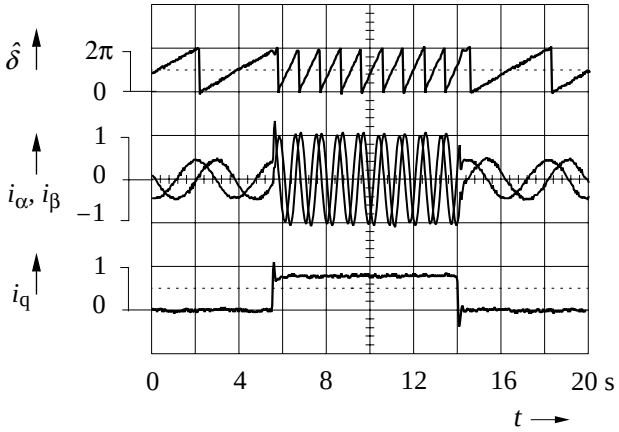

Fig. 15. Constant speed operation at 5 rpm ($f_1 = w_s/2p = \pm 0.16$ Hz), with load step changes of rated magnitude applied.

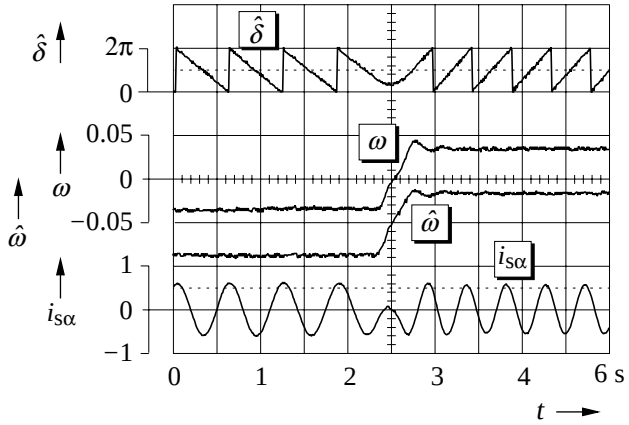

Fig. 17. Reversal of speed between the setpoint values $\omega = \pm 0.04$; torque is constant at 50% nominal value.

speed is maintained without excursions. Dynamic operation at very low speed is demonstrated by Fig. 14, showing a reversal of speed from –10 rpm to +10 rpm ($f_s = \omega_s/2\pi = \pm 0.33$ Hz). The recorded components $\psi_{s\alpha}$ and $\psi_{s\beta}$ of the estimated stator flux linkage vector exhibit sinusoidal waveforms without offset, drift or distortion, and smooth speed operation is achieved. Fig. 15 shows the response to load step changes of rated magnitude while the speed is maintained constant at 5 rpm. This corresponds to operating at a stator frequency of 0.16 Hz ($\omega_s = 0.0032$) during the no-load portions. Fig. 16 shows the low speed performance in a speed reversal process between the set values $\omega = \pm 0.04$. The torque is held constant at a constant value such that the drive operates in the generating mode while the speed is negative. Finally, the performance of the stator resistance identification scheme is demonstrated in Fig. 17. The stator resistance is increased by 30% in a step change fashion. The disturbance causes a sudden deviation from the correct field angle, which produces a wrong value i_q. The new value of r_s is identified after a short delay, and i_q readjusts to its original level. The speed remains unaffected.

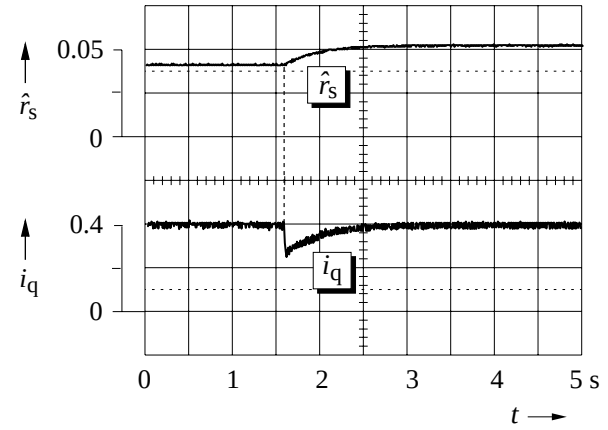

Fig. 16. Identification of the stator resistance, demonstrated by a 30% step increase of the resistance value

5. Summary

Physical limits make sensorless speed control at zero stator frequency impossible when using the fundamental field representation of the induction motor for modeling. Also in the neighborhood of zero stator frequency is speed estimation a problem. Noise, offset, drift, unbalances, bandwidth limits and model parameter mismatch dominate the acquired signals which leads to speed oscillations and instabilities. The fundamental field model is nevertheless very attractive as even highly sophisticated control and identification algorithms can be economically implemented in modern signal processing hardware.

Making use of this situation, more accurate models of the system components are introduced in this paper. An inverter model serves to compensate the nonlinear distortions introduced by the power devices, enabling a more accurate estimation of the stator flux linkage vector. To increase the bandwidth of flux estimation, the stator flux linkage vector is obtained by pure integration. This implies that the time-varying disturbances are compensated by an estimated offset voltage vector. Finally, a stator resistance estimation scheme serves to make the machine model more accurate.

The effectiveness of these methods is demonstrated by experiments. Excellent steady-state and dynamic performance is achieved even at extreme low speed down to 0.003 p.u.

6. References

1. K. Rajashekara (Editor), „Sensorless Control of AC Motors", *IEEE Press Book*, 1996.
2. J. Holtz, „State of the Art of Controlled AC Drives without Speed Sensor", *International Journal of Electronics*, Vol. 80, No. 2, 1996, pp. 249-263.
3. J. Holtz, „The Representation of AC Machine Dynamics by Complex Signal Flow Graphs", *IEEE Transactions on Industrial Electronics*, Vol. 42, No. 3, 1995, pp. 263-271.
4. T. Ohtani, N. Takada, and K. Tanaka, „Vector Control of Induction Motor without Shaft Encoder", *IEEE Transactions on Industry Applications*, Vol. 28, No. 1, 1992, pp. 157-165.
5. M.-H. Shin, D.-S. Hyun, S.-B. Cho and S.-Y. Choe, „An Im-

proved Stator Flux Estimation for Speed Sensorless Stator Flux Orientation Control of Induction Motors", *IEEE Transactions on Power Electronics*, Vol. 15, No. 2, 2000, pp. 312-318.

6. J. Hu and B. Wu, „New Integration Algorithms for Estimating Motor Flux over a Wide Speed Range", *IEEE Transactions on Power Electronics*, Vol. 13, No. 5, 1998, pp. 969-977.
7. X. Xu and D. W. Novotny, „Implementation of Direct Stator Flux Oriented Control on a Versatile DSP Based System", *IEEE Transactions on Industry Applications*, Vol. 29, No. 2, 1991, pp. 694-700.
8. K. Akatsu and A. Kawamura, „Sensorless Very Low-Speed and Zero-Speed Estimations with Online Rotor Resistance Estimation of Induction Motor without Signal Injection", *IEEE Transactions on Industry Applications*, Vol. 36, No. 3, 2000, pp. 764-771.
9. D.-W. Chung and S.-K. Sul, „Analysis and Compensation of Current Measurement Error in Vector-Controlled AC Motor Drives", *IEEE Transactions on Industry Applications*, Vol. 34, No. 2, 1998, pp. 340-345.
10. I.-J. Ha and S.-H. Lee, „An Online Identification Method for both Stator and Rotor Resistances of Induction Motors without Rotational Transducers", *IEEE Trans. on Industrial Electronics*, Vol. 47, No. 4. 2000, pp. 842-853.
11. M. Depenbrock, „Speed Sensorless Control of Induction Motors at Very Low Stator Frequencies", *European Conference on Power Electronics and Applications*, 1999.
12. J.-W. Choi and S.-K. Sul, „Inverter Output Voltage Synthesis using Novel Dead Time Compensation", *IEEE Transactions on Power Electronics*, Vol. 11, No. 2, 1996, pp. 221-224.
13. Y. Murai, T. Watanabe and H. Iwasaki, „Waveform Distortion and Correction Circuit for PWM Inverters with Switching Lag-Times", *IEEE Transactions on Industry Applications*, Vol. IA-23, No. 5, Sept./Oct. 1987, pp. 881-886.